# ARTICLE

# A Preclinical Population Pharmacokinetic Model for Anti-CD20/CD3 T-Cell-Dependent Bispecific Antibodies

Gregory Z. Ferl*, Arthur Reyes, Liping L. Sun, Melissa Cheu, Amy Oldendorp, Saroja Ramanujan and Eric G. Stefanich

CD20 is a cell-surface receptor expressed by healthy and neoplastic B cells and is a well-established target for biologics used to treat B-cell malignancies. Pharmacokinetic (PK) and pharmacodynamic (PD) data for the anti-CD20/CD3 T-cell-dependent bispecific antibody BTCT4465A were collected in transgenic mouse and nonhuman primate (NHP) studies. Pronounced nonlinearity in drug elimination was observed in the murine studies, and time-varying, nonlinear PK was observed in NHPs, where three empirical drug elimination terms were identified using a mixed-effects modeling approach: i) a constant nonsaturable linear clearance term (7 mL/day/kg); ii) a rapidly decaying time-varying, linear clearance term ($t_{1/2}$ = 1.6 h); and iii) a slowly decaying time-varying, nonlinear clearance term ($t_{1/2}$ = 4.8 days). The two time-varying drug elimination terms approximately track with time scales of B-cell depletion and T-cell migration/expansion within the central blood compartment. The mixed-effects NHP model was scaled to human and prospective clinical simulations were generated.
Clin Transl Sci (2018) 11, 296–304; doi:10.1111/cts.12535; published online on 19 January 2018.

**Study Highlights**

**WHAT IS THE CURRENT KNOWLEDGE ON THE TOPIC?**
✔ Linear, time-varying pharmacokinetics of bivalent anti-CD20 monoclonal antibodies that target and deplete B cells have been well characterized in preclinical and clinical studies.

**WHAT QUESTION DID THIS STUDY ADDRESS?**
✔ How can time-varying, nonlinear pharmacokinetic profiles of an anti-CD20/CD3 bivalent monoclonal antibody in cynomolgus monkey be characterized with respect to changes in on-treatment B- and T-cell dynamics and scaled to human?

**WHAT THIS STUDY ADDS TO OUR KNOWLEDGE**
✔ This study provides a mixed-effects modeling framework for description of time-varying, nonlinear drug pharmacokinetics associated with bivalent anti-CD20/CD3 antibodies and insight into mechanistic drivers of drug PK.

**HOW THIS MIGHT CHANGE CLINICAL PHARMACOLOGY OR TRANSLATIONAL SCIENCE**
✔ Understanding of the relationship between time-varying and nonlinear drug pharmacokinetics and baseline B- and T-cell counts will increase the accuracy of projected human pharmacokinetic profiles based on preclinical PK data. Furthermore, variability in drug pharmacokinetics across patients with different baseline tumor characteristics can be more accurately assessed.

BTCT4465A is a full-length, fully humanized immunoglobulin G1 (IgG1) T-cell-dependent bispecific (TDB) antibody for the treatment of B-cell malignancies.[1] One arm binds specifically to CD3 on T-cells and the other to CD20 present on normal and neoplastic B-cells. Simultaneous binding of both arms to their respective targets facilitates T-cell-mediated killing of CD20+ B-cells as demonstrated by *in vitro* and *in vivo* data.[1] The therapeutic potential of this approach has been established in clinical trials of blinatumomab,[2] a bispecific T-cell engager (BiTE) targeting CD19 that was approved in 2014 by the US Food and Drug Administration for the treatment of relapsed/refractory B-cell acute lymphoblastic leukemia (ALL). However, the structural differences between the BiTE format, a 55 kDa fusion protein composed of two single-chain antibodies (scFvs)[3] and the full-length 150 kDa BTCT4465A bispecific antibody that includes the half-life regulating Fc region, leads to significant

differences in the pharmacokinetics (PKs) of these molecules. Whereas rapid plasma clearance of the BiTE (elimination half-life = 2.11 ± 1.42 h) necessitates constant intravenous infusion (4–8 weeks per cycle),[4] BTCT4465A is intended for intermittent infusions (several hours per cycle).

Initial studies with BTCT4465A in mice and nonhuman primates (NHPs, cynomolgus monkeys),[1] suggested that nonlinear target-mediated clearance via CD3- and CD20-expressing cells may be an important mechanism of drug disposition. The two target molecules are abundant in immunocompetent animals and may serve as a primary mechanism for target-mediated drug disposition and nonlinear plasma PKs. Clinically, monospecific, bivalent anti-CD20 monoclonal antibodies, including rituximab,[5] obinutuzumab,[6] ocrelizumab, and ofatumumab,[7] exhibit linear, time-varying elimination in oncology indications, where total drug clearance decreases as B-cells are depleted. Likewise, the
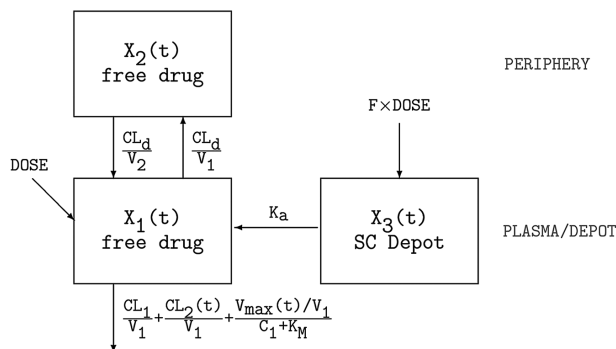
**Figure 1** Schematic representation of an augmented two-compartment PK model with subcutaneous absorption, where $X_1(t)$ is the central plasma compartment and $X_2(t)$ represents peripheral tissue, both using units drug in $\mu$g. $X_3(t)$ represents the subcutaneous (s.c.) depot used for describing s.c. dosing. $CL_1$ and $V_1$ represent linear, nonsaturable drug clearance and central volume of distribution. $CL_d$ and $V_2$ represent distribution clearance and peripheral tissue volume of distribution. $K_a$ represents the fractional absorption rate of drug from the s.c. depot (1/time) and F is fractional bioavailability ($0 \leq F \leq 1$). $CL_2(t)/V_1$ and $(V_{max}(t)/V_1)/(C_1 + K_M)$ are ostensibly correlated with fractional B-cell and T-cell–mediated drug disposition/elimination, respectively, where $CL_2(t) = CL_2^0 \cdot e^{-\lambda_2 t}$ and $V_{max}(t) = V_{max}^0 e^{-\lambda_1 t}$.

anti-CD3 monoclonal antibody otelixizumab,[8] exhibits nonlinear, but not time-varying, elimination in patients treated for psoriasis and type 1 diabetes.

In this study we examined data from seven NHP safety and PK studies in addition to pharmacokinetic/pharmacodynamic (PK/PD) studies performed in transgenic mice expressing human CD3 and CD20 on T- and B-cells, respectively. Collected NHP PK data were kinetically analyzed by fitting a population model (**Figure 1** and Eqs. (1)–(3)) to the data in order to characterize time-dependent antibody catabolism, estimate population PK parameters, and compare them to previously published empirical population models of anti-CD20 mAbs.

## METHODS
### PK/PD studies in mice
All *in vivo* experimental procedures were approved by Genentech's Institutional Animal Care and Use Committee. Human CD20-human CD3 double-transgenic mice were produced by crossing mice containing each of the two single transgenes.[9,10] Twelve mice per group were administered a single intravenous (i.v.) bolus dose of vehicle or BTCT4465A (0.005–0.5 mg/kg). Serum was collected at selected timepoints and stored at –70°C until measured using an enzyme-linked immunosorbent assay (ELISA) to determine the amount of BTCT4465A in the serum. All mouse data analyzed here were previously reported in Sun *et al.*[1]

### PK/PD studies in nonhuman primates
All NHP studies were conducted at Charles River Laboratories (Reno, NV) using purpose-bred, naive, cynomolgus monkeys of Chinese origin. For the single-dose studies, three or four cynomolgus monkeys were administered a single slow bolus (approximated as an instantaneous bolus injection in the model) i.v. dose of BTCT4465A (0.001–1 mg/kg). For

the repeat dose studies, three to eight cynomolgus monkeys were administered a 1 mg/kg subcutaneous dose, slow bolus intravenous dose or 1-h infusion of BTCT4465A (0.01–1 mg/kg) once weekly for a total of four doses. For all studies, serum was collected at selected timepoints and stored at –70°C until measured using an ELISA assay with a 1.6–3 ng/mL limit of quantification to determine the amount of BTCT4465A in serum. PK samples that tested positive for antidrug antibodies (ADAs) by an ELISA assay were excluded from analysis. Note that drug immunogenicity is not studied in depth here since ADA responses do not translate well from NHP to human.[11,12] Two of the seven NHP studies analyzed here were previously reported in Sun *et al.*[1]

### Compartmental model structure for murine and nonhuman primate PK data
All data in this study were analyzed using a two-compartment PK model with first-order subcutaneous absorption augmented with a time-varying, nonlinear Michaelis–Menten clearance term ($V_{max}^0$, $\lambda_1$, $K_M$) and a time-varying, linear clearance term ($CL_1$, $CL_2^0$, $\lambda_2$), as shown in **Figure 1**, with equations written as follows:

$$\frac{dX_1(t)}{dt} = u_{IV}\delta(t) + \frac{CL_d}{V_2}X_2(t) - \frac{CL_1 + CL_2^0 e^{-\lambda_2 t} + CL_d}{V_1}X_1(t)$$
$$- \frac{V_{max}^0 \, e^{-\lambda_1 t}}{\frac{X_1(t)}{V_1} + K_M} \cdot \frac{X_1(t)}{V_1} + K_a X_3(t) \tag{1}$$

$$\frac{dX_2(t)}{dt} = \frac{CL_d}{V_1}X_1(t) - \frac{CL_d}{V_2}X_2(t) \tag{2}$$

and

$$\frac{dX_3(t)}{dt} = F \cdot u_{sc}\delta(t) - K_a X_3(t) \tag{3}$$

where $X_1$, $X_2$, and $X_3$ represent amount of drug ($\mu$g); $u_{IV}$ and $u_{sc}$ are amounts of drug ($\mu$g) administered to the central (i.v.) or subcutaneous (s.c.) compartment. Six variants of the compartmental model described by Eqs. (1)–(3) were evaluated (**Table 1**), representing different combinations of the three plasma clearance terms in **Figure 1**. Model parameters are described in **Table 2**. Software and computational methods are described in the **Supplementary Information**.

### Mixed-effects and covariate analysis of nonhuman primate data
Analysis of plasma PK data collected from cynomolgus monkeys was conducted using the mixed-effects (population) modeling approach[13,14] in order to estimate (i) mean PK parameters across all animals, and (ii) intersubject variability between estimated PK model parameters. We also assessed the impact of body weight, antibody cell line source (CHO vs. *E. coli*-derived), and baseline T- and B-cell levels as covariates on model parameters. We excluded from analysis those drug plasma concentrations that might have been impacted by the presence of antidrug antibodies, i.e., ADA-positive PK samples. However, in addition to estimating mean PK

**Table 1** Comparison of drug elimination parameter estimates based on cynomolgus monkey PK data and final objective function value (OFV) for six base model variants without covariates considered in this study (cf. **Figure 1**)

| Clearance mechanism (all include $CL_1$) | Variant | $V_{max}(t)$ | $K_M$ | $CL(t)$ | OFV | $N_p$ |
|---|---|---|---|---|---|---|
| — | I | — | — | 7.6 | 166 | 2 |
| Constant $V_{max}$ | II | 444 | 6.1 | 0.16 | 9.86 | 5 |
| Time-varying $CL$ | III | — | — | $7.3 + 23e^{-0.19t}$ | −136 | 5 |
| Time-varying $V_{max}$ | IV | $2171e^{-0.21t}$ | 25 | 7.4 | −148 | 6 |
| Constant $V_{max}$ + Time-varying $CL$ | V | 315 | 9.9 | $2.9 + 18e^{-0.28t}$ | −155 | 8 |
| Time-varying $V_{max}$ + Time-varying $CL$ | VI | $1280e^{-0.144t}$ | 19.6 | $7.05 + 63.8e^{-10.1t}$ | −168 | 9 |

For this analysis $CL_2(t)$ and $V_{max}(t)$ are defined as $CL(t) = CL_1 + CL_2^0 e^{-\lambda_2 t}$ and $V_{max}(t) = V_{max}^0 e^{-\lambda_1 t}$. Units are listed in **Table 2**. The objective function used here is proportional to −2 log-likelihood such that ΔOFV of 6.63/9.21/11.3 are considered statistically significant ($P \sim 0.01$) outcome of the likelihood-ratio test with one/two/three degree(s) of freedom,[31–33] respectively. Np is the number of parameters, including $\eta$'s (Eq. (4)), in the drug elimination term of each model variant.

parameters across all animals using Eqs. (1)–(3), the mixed-effects approach yielded estimated PK parameters for each individual animal i. Using $CL_1$ as an example, this was written as:

$$CL_1^i = CL_1^{pop} \cdot e^{\eta_i^{CL_1}} \qquad (4)$$

where, $CL_1^i$ is the estimated clearance for animal i. $CL_1$ values across all animals were assumed to be described by a log-normal distribution, where $\eta^{CL_1}$ is a normally distributed random variable and $CL_1^{pop}$ is the mean estimated clearance for the population of animals in the study. The percentage of interindividual variabilities of parameters for which $\eta$ distributions are estimated, typically expressed as apparent percent coefficients of variation (%CV), were calculated as:

$$\%CV_p = \sqrt{\left(e^{\Omega_{ii}^p} - 1\right)} \times 100\% \qquad (5)$$

where, $\Omega_{ii}^p$ corresponds to the diagonal element of the variance–covariance matrix ($\Omega$) corresponding to parameter p.

Covariate analysis was performed using the stepwise covariate model-building method.[15] Body weight and baseline T-/B-cell blood counts were tested as continuous linear and power functions on PK model parameters; cell lines were tested as a categorical covariate. For example, a linear covariate effect of body weight (BW) on $CL_1$, as written in Eq. (4), is written as

$$CL_1^i = CL_1^{pop} e^{\eta_i^{CL_1}} \left(1 + \Theta^{cov} \left(BW_i - \widetilde{BW}\right)\right) \qquad (6)$$

where, $BW_i$ was the body weight of animal i, $\widetilde{BW}$ was the median body weight across all animals, and $\Theta^{cov}$ was a dimensionless parameter characterizing the magnitude of covariate effect. Likewise, a covariate power model is written as:

$$CL_1^i = CL_1^{pop} e^{\eta_i^{CL_1}} \left[\frac{BW_i}{\widetilde{BW}}\right]^{\Theta^{COV}} \qquad (7)$$

Model discrimination analysis was performed by comparing final objective function values (OFVs) for each model, where OFV is proportional to −2 log-likelihood as calculated by NONMEM.[16] Referencing a standard chi-square distribution table, a difference of 6.63, 9.21, or 11.3 between OFVs (ΔOFV) for two different nested models differing by one, two, or three degrees of freedom, respectively, corresponds to a P-value of 0.01 for a null hypothesis that each of the two structures under consideration are statistically equivalent.[16–18]

**Allometric scaling**
NHP (cynomolgus, c) PKs were scaled to humans (h) using the standard allometric equation,[19,20] where for model parameter p,

$$p_h = p_c \left[\frac{BW_h}{BW_c}\right]^b \qquad (8)$$

When generating prospective clinical simulations, $CL_1$ and $CL_d$ values were scaled by body weight with an allometric exponent of b = 0.85[21]; $V_1$ and $V_2$ were scaled by an exponent of b = 1.[21] As an approximation of clinical CD20+ tumor-mediated drug clearance, $CL_2^0$ and $\lambda_2$ were fixed to values estimated for NHL patients treated with rituximab.[5] $V_{max}^0$ was assumed to scale from NHP by body weight, with an exponent of b = 1 and $\lambda_1$ was fixed to the estimated NHP value (**Table 2**).

**RESULTS**
**NHP PK/PD studies**
**Figure 2** shows pooled mouse PK (**Figure 2a**) and per-animal NHP PK measurements (**Figure 2b**) along with the corresponding changes in CD4+, CD8+, and CD20+ cell counts (**Figure 2c**) for NHPs that were given four doses at 1 mg/kg, administered 1 week apart. Dosing rapidly led to a decline (within 1 h) in CD4+ and CD8+ circulating T-lymphocyte numbers. That response was followed by resurgence to levels at or above baseline levels within 48 h. This behavior has been attributed to activation-induced margination of blood lymphocytes to tissues upon dosing followed by re-emergence of activated CD4+ and CD8+ T cells in blood by 48 h. Results of a single dose study are shown in the **Supplementary Information, Figure S1**. In both the single and multidose studies, T-cell counts appeared to be trending towards baseline levels in the weeks after the last dose; however, the number of animals at later timepoints (t > 28 days) was low (n = 4) compared with earlier time-points (n ≥ 25). The study duration was not long enough to permit observation of a complete return to pretreatment T-cell levels (**Figure 2c**). Meanwhile, peripheral blood B-cells

**Table 2** Summary of population model parameters (cf. **Figure 1**) for Model VI

| Parameter | Definition | Units | Pop. Mean | SE | %CV | SE |
|---|---|---|---|---|---|---|
| $K_a$ | Subcutaneous absorption rate | 1/day | 1.33 | 0.23 | — | — |
| $Z$ | Bioavailability = $1/(1 + e^{-Z})$ | dimensionless | 1.66 | 0.56 | — | — |
| $CL_1$ | Nonsaturable mAb elimination | mL/day/kg | 7.05 | 1.4 | 25 | 13 |
| $CL_2^0$ | Initial linear time-varying elimination rate | mL/day/kg | 63.8 | 41 | 82 | 91 |
| $\lambda_2$ | Decay constant for $CL_2$ | 1/day | 10.1 | 8.7 | — | — |
| $CL_d$ | mAb distribution clearance | mL/day/kg | 31.3 | 6.9 | 69 | 15 |
| $V_1$ | Central distribution volume | mL/kg | 44.4 | 3.5 | 41 | 6 |
| $V_2$ | Peripheral distribution volume | mL/kg | 47.3 | 7.2 | 31 | 15 |
| $V_{max}^0$ | Initial nonlinear saturable elim rate | $\mu$g/mL | 1280 | 678 | 41 | 16 |
| $\lambda_1$ | Decay constant for $V_{max}$ | 1/day | 0.144 | 0.048 | — | — |
| $K_M$ | Michaelis−Menten constant | $\mu$g/mL | 19.6 | 10 | — | — |

In a *post hoc* step, $CL_1$, $CL_2^0$, $CL_d$, $V_1$, and $V_2$ were normalized by median body weight (3.12 kg) across all animals. Note that subcutaneous bioavailability = $1/(1 + e^{-Z}) = 0.84$. Pop. Mean, Population Mean; %CV, apparent percent coefficient of variation (interindividual variability); SE, standard error (a measure of precision for fitted population means and apparent percent coefficients of variation).
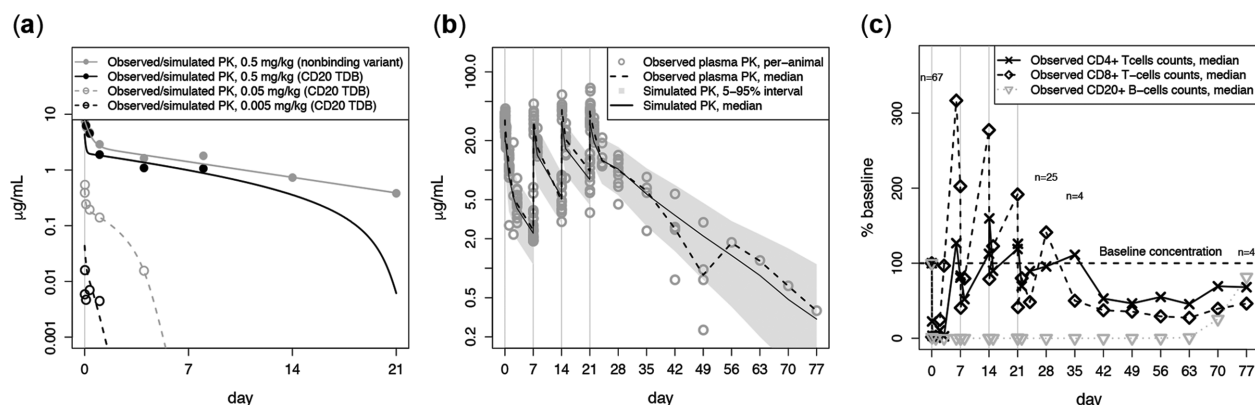


**Figure 2** Murine PK and cynomolgus monkey PK/PD data with model simulations. (**a**) Two-compartment nonlinear PK model, as described by Eqs. (1) and (2), with $CL_2^0 = 0$ and $\lambda_1 = 0$, fitted to murine data. Key estimated parameters for the CD20 TDB are $CL_1 = 16$ mL/day/kg, $K_M = 0.015$ $\mu$g/mL, and $V_{max} = 12$ $\mu$g/day. The solid gray curves indicate model fitted to PK data from the low-affinity CD3 TDB variant UCHT1 [1] ($V_{max}$ fixed to zero). (**b**) Comparison of mixed-effects model simulations (median PK profile and interanimal variability) generated using fitted mixed-effects parameters summarized in **Table 2**, and observed PK data for 1 mg/kg i.v. bolus and slow push repeat dosing cohorts. Solid line and shaded region correspond to simulated median and 5–95% intervals. Circles are observed drug concentrations in plasma and dashed line corresponds to median observations at each timepoint. (**c**) Corresponding changes in median peripheral blood CD4+, CD8+ T-cell counts, and CD20+ B-cell counts. Number of animals (*n*) for which T- and B-cell levels were measured is indicated at t = 0, 28, 35, and 77 days. In all panels, vertical lines indicate dosing times.

were rapidly depleted after dosing, presumably due to T-cell-mediated killing. Peripheral blood B cells showed evidence of recovery ∼7 weeks after the last dose was administered (**Figure 2c**). Tissue B-cell counts may have declined at a slower rate, but they appear to have been nearly depleted 7 days following a 1-mg/kg i.v. dose.[1] B-cell counts appeared to return to baseline levels once serum concentrations of BTCT4465A fell below a threshold of ∼1 nM (0.15 $\mu$g/mL). During repeat i.v. administration of BTCT4465A at 1 mg/kg, the data demonstrated that the total rate of drug elimination (CL) was qualitatively lower during days 21–28 compared with days 0–7 (**Figure 2b**), consistent with time-dependent CL previously described for the anti-CD20 directed monoclonal antibodies rituximab,[5] obinutuzumab,[6] ocrelizumab,[22] and ofatumumab.[7]

**Compartmental model fitted to pooled murine PK data**
**Figure 2a** shows pooled murine data and their fit to the model. A strong nonlinearity in drug elimination with respect

to plasma concentration was apparent from visual inspection, characterized by estimated $K_M$ and constant $V_{max}$ values of 0.015 $\mu$g/mL and 12 $\mu$g/day, respectively. Linear drug elimination CL was estimated to be 16 mL/day/kg (±2 mL/day/kg) for all fits shown. Due to the small amount of data used, numerical precision of $K_M$ and $V_{max}$ was relatively low, with standard errors greater than 0.015 $\mu$g/mL and 12 $\mu$g/day, respectively.

Due to the relatively small amount of PK data collected in the mouse studies, a time-varying $V_{max}$ model was not evaluated. However, a linear PK model ($V_{max} = 0$) was fitted to all pooled murine data (not shown) and compared with nonlinear model fits via the Akaike Information Criterion (AIC),[23] estimated as 0.13 for the final fitted nonlinear model and 0.62 for the final fitted linear model. The lower AIC score of the nonlinear model suggests that it is better than the linear model, consistent with the strong nonlinearity apparent from visual inspection of the data in **Figure 2a**. The solid gray curve represents the model with $V_{max}$ fixed to zero fitted to PK data

collected for UCHT1,[1] a CD20 TDB variant with a very low affinity CD3 arm.

## Mixed-effects model fitted to cynomolgus monkey PK data

Each of the six model variants evaluated in this study were fitted to all available cynomolgus monkey PK data (**Tables 1** and **S1**). The model with time-varying $V_{max}$ and time-varying CL terms (Model VI) yielded the best fit of the model to the data. Model VI had a final OFV of −168 compared with OFV = −155 for the next-best model (Model V), resulting in a statistically significant ($P < 0.001$) $\Delta$OFV of 13.1 between model variants V and VI. The estimated value of $\lambda_2$ (10.1/day) resulted in a rapid decay of $CL_2$, which drops to 50% of its initial value (63.8 mL/day/kg) 1.6 h posttreatment. The estimated value of $\lambda_1$ (0.144/day) resulted in a much slower decay of $V_{max}$, which drops to 50% of its initial value (1,280 $\mu$g/day) 4.8 days posttreatment.

**Table 2** lists the estimated population mean, standard error, and interindividual variability of each parameter included in the final base model (no covariate effects), where percent interindividual variability (apparent %CV) of PK parameters range from 25–69%. Precision of fixed-effects parameters was generally good at less than ~50% relative error (100%·SE/Pop. Mean, **Table 2**); exceptions were $CL_2^0$ and $\lambda_2$, which had slightly higher relative errors of ~65 and 85%, respectively, due to their presumed dependence on target-mediated clearance via rapidly depleting B cells, which was reflected in only a small portion of the data. The estimated variance–covariance matrix for model VI is shown in **Table S2.** Estimates of random effect parameters that describe the distribution of animal-specific $\eta$ values (Eq. (4)) are depicted by the histograms shown in **Figure S2**. Representative per-animal *post hoc* fits of Model VI are shown in **Figure S3** and plots of observed PK values vs. mean/per-animal simulated values and residual plots for Model VI are shown in **Figures S4–S5**.

**Figure 2b** depicts qualitative agreement between the median simulated PK profiles (solid line, median), simulated interanimal variability for repeated Model IV dosing (shaded region, 5–95% confidence interval), and PK samples (circles, individual observations; dashed line, median) obtained from the most data-rich animal cohort (1 mg/kg weekly x 4).

## Comparison of time-varying mAb clearance terms and observed T-/B-cell dynamics in blood

**Figure 3** compares the time course of linear/nonlinear fractional drug elimination (1/day) and measures B-/T-cell dynamics in blood. Qualitatively, the time scale of fractional time-varying, nonlinear drug elimination (**Figure 3a**) tracked with that of total T-cell expansion and trafficking dynamics in blood (**Figure 3c**), where both the nonlinear elimination term and T-cell counts had almost completely decayed to baseline by 28 days. Time to peak elimination from blood via time-varying, nonlinear drug elimination (**Figure 3a**) occurred at ~2 days postinjection, while observed peak T-cell levels in blood occurred at ~7–14 days postinjection. Additionally, across the preclinical range of doses evaluated, a pronounced dose-dependency was observed in both the nonlinear drug elimination term and the T-cell response,

particularly in the first 7 days postdose. Likewise, the time scales of fractional time-varying linear elimination (**Figure 3b**) tracked with the nearly 100% depletion of peripheral blood B cells by 24 h postdose (**Figure 3d**). Dose-dependency of peripheral blood B-cell depletion could not be detected in the preclinical studies, possibly due to the bulk of B-cell depletion occurring prior to the first sampling timepoint at 2 h postdose.

## Covariate analysis

The base population PK model for NHP provided a reasonable description of the observed data (**Figure 2b**). Nonetheless, an exploratory covariate analysis was conducted to assess potential relationships between (i) each model parameter and (ii) body weight, baseline CD4+ T–, CD8+ T–, and CD20+ B-cell blood counts and the source of drug. Statistically significant ($P < 0.005$) continuous linear (Eq. (6)) and categorical (*E. coli*- vs. CHO-derived material) covariates were identified and are summarized in **Table S3**. No continuous power model covariates (Eq. (7)) were identified. Per-animal estimates of linear, nonsaturable clearance ($CL_1$) were compared for the drug derived from each source. Qualitative inspection of estimated $CL_1$'s across all animals (**Supplementary Information, Figure S6**) suggests that there is little difference in constant, nonsaturable drug elimination mechanisms for *E. coli*- vs. CHO cell-derived drug. The drug source was also included as a categorical covariate but did not appear to significantly impact the rate of elimination clearance ($CL_1$); however, a statistically significant covariate effect of cell source was observed on central volume of distribution ($V_1$), distribution clearance ($CL_d$), and the linear, time-varying clearance term ($CL_2^0$). Generally, cell source effects on estimated model parameters may be confounded by interstudy variability, since only two of the seven NHP cohorts received CHO cell-derived mAb. Additional identified covariate relationships included effects of body weight on $\lambda_2$ as well as baseline CD4+ T-cell counts on $CL_1$ and $\lambda_1$. Estimated interindividual variabilities (%CVs) for the full model with covariates were ~20, 50, 15, and 5% lower for $CL_1$, $CL_2^0$, $CL_d$, and $V_1$, respectively, compared with the base model (**Supplementary Information, Table S3**). $\eta$ shrinkages are summarized in the **Supplementary Information, Table S4.** The full model with covariates resulted in a lower OFV (–324 vs. –168) and an overall improved fit of model to data (**Supplementary Information, Figure S7**).

## Model-predicted human plasma PK

**Figure 4** shows projected mean human PK, using the final model with covariates scaled by Eq. (8). Monthly dosing was simulated at 1, 10, and 100 mg flat dosing, where $C_{max}$ at steady state (5th dosing cycle) is linear at 0.37, 3.7, and 37 $\mu$g/mL across the three doses. Accumulation of drug over multiple dosing cycles and decay of the time-varying clearance terms results in an increase in AUC of 268%, 253%, and 169% at steady state compared with AUCs calculated for the first dosing cycle across the 1, 10, and 100 mg dose groups. Likewise, $C_{min}$ is nonlinear across the dose during the first cycle and linear across the dose at steady state (**see Table inset in Figure 4**).
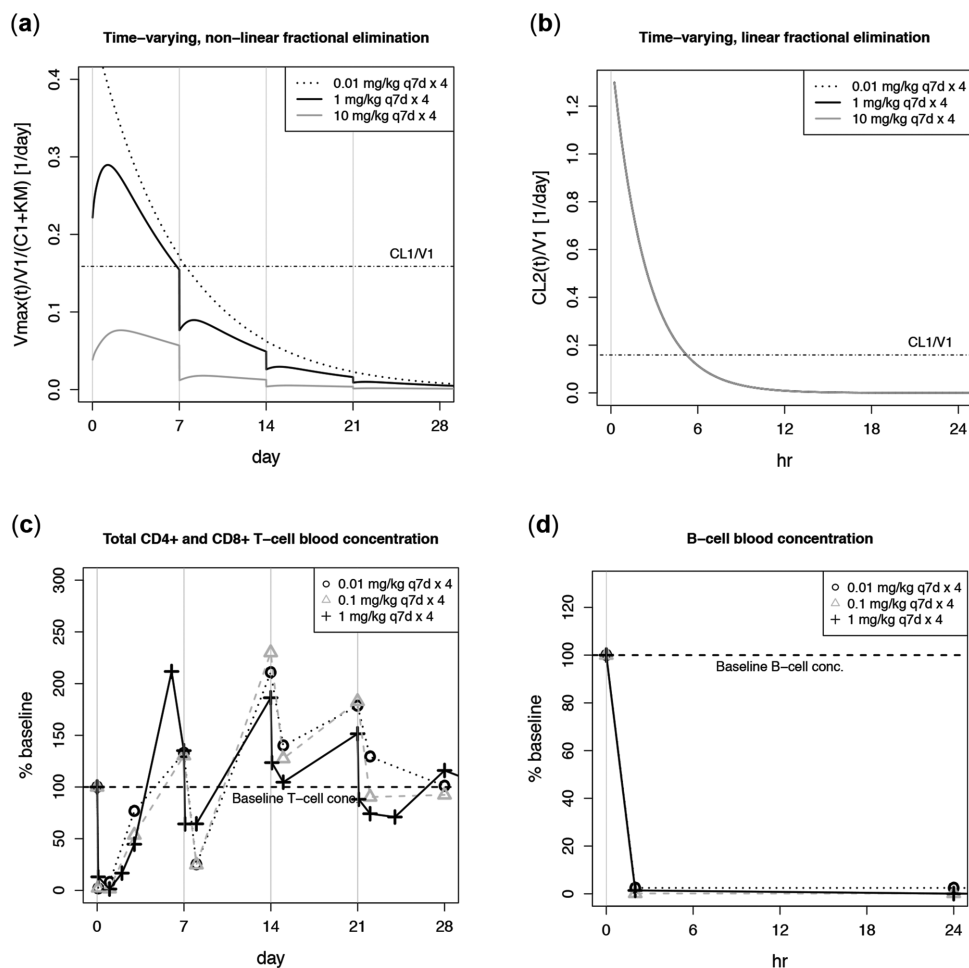
**Figure 3** Simulated fractional drug elimination rates, estimated by the mixed-effects model, illustrate the contribution to total drug clearance of (**a**) time-varying, nonlinear mechanisms and (**b**) time-varying, linear mechanisms. Fractional drug elimination rate via time-invariant, linear mechanisms, constant over the course of the study, is represented by the horizontal line on each panel. Measured (**c**) sum of CD4+ and CD8+ T-cell concentrations in plasma and (**d**) CD20+ B-cell concentrations in plasma are shown for comparison, normalized to measured pretreatment T- and B-cell concentrations. In all panels, vertical lines indicate dosing times.

## DISCUSSION

Here we studied an anti-CD20/CD3 T-cell-dependent bispecific antibody (BTCT4465A) that exhibits nonlinear PK and PD profiles in transgenic mice and healthy nonhuman primates. BTCT4465A binds to CD3 receptors expressed on T cells and CD20 receptors expressed on healthy and neoplastic B cells. Tissue distribution and total expression levels of CD3 and CD20 may change significantly during the course of treatment as CD4+ and CD8+ T-cell populations expand following activation and traffic into peripheral tissues and as B-cell populations are depleted in response to ligation of CD3 and CD20. This dynamic chain of events leads to time-varying, nonlinear drug PK as target-mediated drug elimination via CD3 and CD20 changes with time. The extent to which CD3 and CD20 contribute to drug elimination kinetics may vary depending on total expression level and internalization rates of each receptor. Rapid redistribution and expansion of T cells, cytokine release, and rapid target cell depletion observed with BTCT4465A were

consistent with preclinical (NHP) pharmacodynamic observations of other T-cell-dependent bispecific antibodies (REGN1979),[24] antibody fragments (blinatumomab BiTE),[25] and CD3xCD123 DART[26] in development for treatment of hematological malignancies. PKs of these molecules is dependent on format, with PK of low molecular weight (~50 kDa) BiTE and DART fragments dominated by rapid systemic clearance, while target-mediated elimination is a major driver for the clearance of higher molecular weight (150 kDa) full-length antibodies that undergo FcRn-mediated half-life extension. The PK/PD characteristics of various bispecifc antibody formats has been recently reviewed by Trivedi *et al.*[27]

CD20 is largely a noninternalizing receptor,[28,29] and is the target for several monospecific, bivalent anti-CD20 monoclonal antibodies approved for oncology[5,6,30–33] and other[7,22,32,34,35] indications (**Table 3**). These therapeutics impact the progression of B-cell lymphomas and rheumatoid arthritis (RA) by targeting and depleting CD20+ B lymphocytes. Moreover, B-cell depletion occurs in multiple
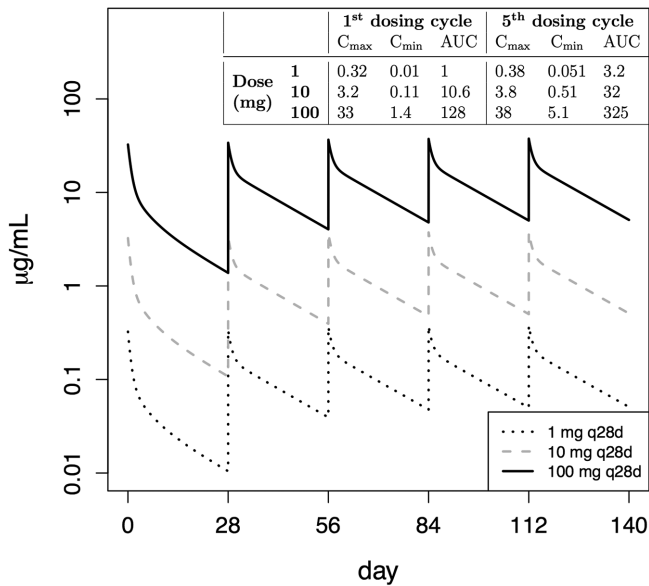
**Figure 4** Projected human (70 kg) plasma PK, scaled from cynomolgus monkeys (3.12 kg). Simulations generated by the final model with covariates scaled from NHP (**Table 2**) to humans, using Eq. (8). Summary statistics are shown within the panel; units for $C_{max}$ and $C_{min}$ are $\mu$g/mL; units for AUC are $\mu$g/mL·day.

sclerosis (MS) patients treated with ocrelizumab.[22] Studies indicate that in addition to $CL_1$, a time-varying clearance term ($CL = CL_1 + CL_2 e^{-\lambda_2 t}$) is required when describing PK data obtained in oncology trials, including non-Hodgkin's lymphoma (NHL), chronic lymphocytic leukemia (CLL), and follicular lymphoma (FL). The time-varying term ($CL_2 e^{-\lambda_2 t}$) is not required (or is very small) when evaluating PK models in other application, i.e., RA and MS. For rituximab in NHL and CLL, the initial value of the time-varying clearance term ($CL_2^0$) is high (18 and 8.36 mL/day/kg) compared with the constant clearance term ($CL_1$), which is 2.44 and 1.97 mL/day/kg; the half-lives of $CL_2$ are 30 and 15 days for

NHL and CLL populations, respectively.[5] For obinutuzumab in CLL and FL, the initial values of $CL_2^0$ are also higher (3.3–4.92 and 2.75–4.1 mL/day/kg, respectively) than $CL_1$, which are 1.19–1.45 and 0.99–1.2 mL/day/kg, respectively.[6] Further illustrating the relationship between the rate of target-mediated drug elimination and tumor burden, baseline tumor size (BSIZ) in CLL patients was previously identified by Gibiansky *et al.* as a categorical covariate, where the half-lives of $CL_2$ were 19 and 14 days for CLL and FL patients, respectively, with a high BSIZ ($>$1,750 mm$^2$) and 7 days for patients with a low BSIZ ($\leq$1,750 mm$^2$).[6] Conversely, for rituximab in RA, the time-varying clearance term was evaluated but found to not improve the model's fit to the data and thus was dropped from the final analysis.[35] For ocrelizumab in MS, the initial value of $CL_2^0$ is low (0.714 mL/day/kg) compared with $CL_1$, which is 2.43 mL/day/kg; the half-life of $CL_2$ is relatively long at 231 days.[36] Similar to rituximab, population modeling analysis of ofatumumab for RA and CLL revealed that time-varying clearance was not required to describe PK data from RA patients.[32] A slightly different, more mechanistic modeling approach was taken for the CLL population, where a target-mediated disposition (TMD) model that explicitly included B-cell counts and irreversible binding was implemented such that the drug elimination rate decreased as B cells were depleted.[32]

A clear trend emerged when we compared population modeling analyses across these four molecules (rituximab, obinutuzumab, ocrelizumab, and ofatumumab) and five therapeutic indications (NHL, CLL, RA, FL, and MS). Significant time-varying clearance (defined here as $CL_2^0 > CL_1$) was apparent only in oncology indications, where CD20+ cell counts in patients with B-cell malignancies are typically much higher than in other indications. The only nononcologic indication with an identifiable time-varying drug elimination term was ocrelizumab for MS. However, in this case, $CL_2^0$ was smaller than $CL_1$ and had a much longer half-life than $CL_2^0$ as estimated in oncology studies, and may reflect the absence of an initial, rapid reduction in neoplastic B-cell levels. Furthermore, in obinutuzumab treatments for CLL and FL, the

**Table 3** Estimated population mean linear and nonlinear clearance rates from published clinical pharmacokinetic studies of monospecific, bivalent anti-CD20 mAbs compared with cynomolgus monkey PK parameters estimated here for BTCT4465A bispecific CD20/CD3 mAb and scaled to humans

| Molecule | Indication | $CL_1$ | $CL_2^0$ | $\lambda_2$ | Reference |
|---|---|---|---|---|---|
| Rituximab | NHL | 2.44 | 18.0 | 0.023 | Li[5] |
| Rituximab | CLL | 1.97 | 8.36 | 0.046 | Li[5] |
| Rituximab | RA | 3.68 | ~0 | ~0 | Ng[22] |
| Obinutuzumab | CLL | 1.19/1.45 (F/M) | 3.3/4.92 (F/M) | 0.036 (hi BSIZ) | Gibiansky[6] |
| Obinutuzumab | CLL | 1.19/1.45 (F/M) | 3.3/4.92 (F/M) | 0.095 (lo BSIZ) | Gibiansky[6] |
| Obinutuzumab | FL | 0.99/1.2 (F/M) | 2.75/4.1 (F/M) | 0.047 (hi BSIZ) | Gibiansky[6] |
| Ocrelizumab | MS | 2.43 | 0.714 | 0.0030 | PI[23] |
| Ofatumumab | RA | 2.57 | ~0 | ~0 | Struemper[19] |
| Ofatumumab | CLL | 2.57 | n/a (TMD) | n/a (TMD) | Struemper[19] |
| BTCT4465A | Preclinical | 3.2–4.4[a] | not scaled | not scaled | — |

[a]Scaled to human.

Units for $CL_1$ and $CL_2^0$ are mL/day/kg and units for $\lambda_2$ are 1/day, where total antibody clearance is written as $CL(t) = CL_1 + CL_2^0 \cdot e^{-\lambda_2 t}$. Note that the published values of $CL_1$ and $CL_2^0$ are expressed in units of mL/day, divided here by a nominal average body weight of 70 kg. Estimated cynomolgus monkey clearance values for BTCT4465A (**Table 2**) are scaled to human body weight with fixed scaling exponents of 0.75–0.85, where 0.75 is the nominal value used for interspecies scaling of antibody clearance and 0.85 has been identified as optimal for scaling linear antibody PK from cynomolgus monkey to human.[36] Interspecies scaling was not applied to the fitted $\lambda_2$ value for BTCT4465A. M, male; F, female; BSIZ, baseline tumor size; NHL, non-Hodgkin's lymphoma; CLL, chronic lymphocytic leukemia; RA, rheumatoid arthritis; FL, follicular lymphoma; MS, multiple sclerosis.

half-life of $CL_2$ in patients with high baseline tumor loads was longer (14–19 days) than for patients with low baseline tumor loads (7 days), which may reflect a longer initial depletion phase in patients with higher baseline tumor loads. Across all of these studies, binding of the drug to CD20 may represent both distribution as drug exits the plasma compartment via binding, and drug elimination upon lysis of drug-bound B cells. The relationship between patient T-cell levels and target-mediated elimination of anti-CD3 mAbs is not as well understood. However, the clinical PK of anti-CD3 mAb otelixizumab has been demonstrated to be consistent with a nonlinear ($V_{max}$, $K_M$) mechanism of drug elimination.[8]

In population modeling analysis of BTCT4465A, we identified a linear time-varying term ($CL_2^0$, $\lambda_2$), along with a nonlinear, time-varying term ($V_{max}^0$, $K_M$, $\lambda_1$). The rapid decay of $CL_2$ ($t_{1/2} = 1.6$ h) is consistent with observed rapid B-cell elimination from the central blood compartment in healthy NHPs. However, the relatively high $CL_2^0$ value suggests that the linear, time-varying term may reflect other mechanisms in addition to CD20-mediated drug disposition such as rapid initial CD3-mediated drug disposition. The nonlinear, time-varying term may, in part, reflect CD3+ T-cell-mediated drug disposition because blood B cells are depleted within the first 24 h of each NHP study (**Figure 3**). However, B cells in peripheral tissues may continue to impact target-mediated drug elimination at later times (t > 1 day) because B-cell depletion in these compartments is not as rapid or complete compared with blood. As is the case with monospecific, bivalent anti-CD20 mAb, one-armed binding of BTCT4465A to CD3 and/or CD20 may serve as both a distribution term and a drug elimination term as B cells are lysed and the mAb–CD3 complex is internalized by T cells.

Exploratory covariate analyses suggest that body weight, baseline T-cell blood counts, and the drug source (cell line) may be significantly correlated with PK model parameters (**Supplementary Information, Table S3**). Baseline T-cell blood counts were identified as statistically significant covariates on $CL_1$ and $\lambda_1$ (half-life of $V_{max}$); correlation of baseline CD4+ T-cell counts with these two parameters suggests that T-cell-mediated drug disposition is reflected in both saturable and nonsaturable elimination terms of the model. The cell line source of mAb appears to have a covariate effect on distribution clearance and central distribution volume, where $CL_d$ and $V_1$ are lower for *E. coli*-derived material. A significant covariate effect of cell line on linear, time-varying drug elimination ($CL_2^0$) was also observed, where the magnitude of the drug elimination pathway was reduced in CHO-derived mAb. Most CHO-derived mAb PK data were collected in a single large NHP study ($n = 44$), raising the possibility that apparent cell line covariate effects are confounded by interstudy variability. Finally, a covariate effect of body weight on $\lambda_2$ was identified. The fitted population PK model with covariates yielded a significant reduction in objective function value ($-324$ vs. $-168$), and an improved model fit to the data (**Supplementary Information, Figure S7**).

The population model fitted to NHP was scaled to humans so that prospective clinical PK simulations could be generated (**Figure 4**). In humans, the constant, linear clearance term ($CL_1$) is projected to be $\sim$3.2–4.4 mL/day/kg

(**Table 3**), which overlaps with the range of $CL_1$ values for the monospecific, bivalent anti-CD20 mAb considered here ($\sim$1–3.7 mL/day/kg). The remaining time-varying clearance terms in the scaled model utilized previously estimated B-cell-mediated drug disposition rates[5] and T-cell-mediated drug disposition rates estimated here were based on NHP PK data. The resulting simulations (**Figure 4**) indicate that time-varying clearance can be expected across a dose range of 1−100 mg once per month. Additionally, covariate analysis suggests that higher baseline T-cell counts may be significantly correlated with faster drug elimination within the range of doses evaluated (**Supplementary Information, Figure S8**). Note that these prospective clinical simulations are based primarily on data collected in healthy cynomolgus monkeys. The model deconvolutes the complex observed preclinical PK into different kinetic subprocesses with differential time-dependent contributions. This helps us understand the behaviors potentially underlying the complex PK, as discussed above, and sets expectations for clinical observations. However, because of the empirical nature of the model, nonlinear and time-varying parameters ($K_M$, $V_{max}^0$, $CL_2^0$, $\lambda_1$, $\lambda_2$) should not be extrapolated to the human setting without further validation of model based on clinical PK data and have thus far not been used to inform clinical trial design.

## CONCLUSION

In conclusion, a preclinical mixed-effects model that can be scaled to humans has been developed to describe the PK of a bispecific mAb that binds to both CD20 on B cells and CD3 on T cells. Each cell type exhibits a distinct response to treatment, such that peripheral blood B cells are rapidly depleted and T cells undergo rapid expansion and subsequent trafficking to peripheral tissues. The impact of this complex dynamic on drug elimination was captured empirically via kinetically fast and slow time-varying terms within the model, putatively corresponding to B- and T-cell-mediated drug elimination. The resulting model provides a framework for further investigation into the PKs of T-cell-dependent bispecific antibodies. Specifically, applications of this model include facilitating preclinical drug comparability studies following changes in material and scaling of NHP PK to humans based in part on interspecies differences in B- and T-cell levels.

1. Sun, L.L. *et al.* Anti-CD20/CD3 T cell-dependent bispecific antibody for the treatment of B cell malignancies. *Sci. Transl. Med.* **7**, 287ra270 (2015).

2. Topp, M.S. *et al.* Phase II trial of the anti-CD19 bispecific T cell-engager blinatumomab shows hematologic and molecular remissions in patients with relapsed or refractory B-precursor acute lymphoblastic leukemia. *J. Clin. Oncol.* **32**, 4134–4140 (2014).

3. Nagorsen, D., Kufer, P., Baeuerle, P.A. & Bargou, R. Blinatumomab: A historical perspective. *Pharmacol. Ther.* **136**, 334–342 (2012).

4. Zhu, M. *et al.* Blinatumomab, a bispecific T-cell engager (BiTE((R))) for CD-19 targeted cancer immunotherapy: Clinical pharmacology and its implications. *Clin. Pharmacokinet.* **55**, 1271–1288 (2016).

5. Li, J. *et al.* Population pharmacokinetics of rituximab in patients with chronic lymphocytic leukemia. *J. Clin. Pharmacol.* **52**, 1918–1926 (2012).

6. Gibiansky, E. *et al.* Population pharmacokinetics of obinutuzumab (GA101) in chronic lymphocytic leukemia (CLL) and non-Hodgkin's lymphoma and exposure-response in CLL. *CPT Pharmacometrics Syst. Pharmacol.* **3**, e144 (2014).

7. Ostergaard, M. *et al.* Ofatumumab, a human anti-CD20 monoclonal antibody, for treatment of rheumatoid arthritis with an inadequate response to one or more disease-modifying antirheumatic drugs: Results of a randomized, double-blind, placebo-controlled, phase I/II study. *Arthritis Rheum.* **62**, 2227–2238 (2010).

8. Wiczling, P., Rosenzweig, M., Vaickus, L. & Jusko, W.J. Pharmacokinetics and pharmacodynamics of a chimeric/humanized anti-CD3 monoclonal antibody, otelixizumab (TRX4), in subjects with psoriasis and with type 1 diabetes mellitus. *J. Clin. Pharmacol.* **50**, 494–506 (2010).

9. de la Hera, A., Muller, U., Olsson, C., Isaaz, S. & Tunnacliffe, A. Structure of the T cell antigen receptor (TCR): Two CD3 epsilon subunits in a functional TCR/CD3 complex. *J. Exp. Med.* **173**, 7–17 (1991).

10. Gong, Q. *et al.* Importance of cellular microenvironment and circulatory dynamics in B cell immunotherapy. *J. Immunol.* **174**, 817–826 (2005).

11. Ponce, R. *et al.* Immunogenicity of biologically-derived therapeutics: assessment and interpretation of nonclinical safety studies. *Regul. Toxicol. Pharmacol.* **54**, 164–182 (2009).

12. van Meer, P.J. *et al.* Immunogenicity of mAbs in nonhuman primates during nonclinical safety assessment. *MAbs.* **5**, 810–816 (2013).

13. Sheiner, L.B. & Beal, S.L. Evaluation of methods for estimating population pharmacokinetics parameters. I. Michaelis-Menten model: routine clinical pharmacokinetic data. *J. Pharmacokinet. Biopharm.* **8**, 553–571 (1980).

14. Sheiner, L.B. & Beal, S.L. Evaluation of methods for estimating population pharmacokinetic parameters. II. Biexponential model and experimental pharmacokinetic data. *J. Pharmacokinet. Biopharm.* **9**, 635–651 (1981).

15. Jonsson, E.N. & Karlsson, M.O. Automated covariate model building within NONMEM. *Pharm. Res.* **15**, 1463–1468 (1998).

16. Bonate, P.L. *Pharmacokinetic-Pharmacodynamic Modeling and Simulation* (Springer, New York, 2011).

17. Beyer, W.H. *CRC Standard Mathematical Tables* (Chemical Rubber Co., Florida, 1978).

18. Wahlby, U., Bouw, M.R., Jonsson, E.N. & Karlsson, M.O. Assessment of type I error rates for the statistical sub-model in NONMEM. *J. Pharmacokinet. Pharmacodyn.* **29**, 251–269 (2002).

19. Adolph, E.F. Quantitative relations in the physiological constitutions of mammals. *Science.* **109**, 579–585 (1949).

20. Dedrick, R.L. Animal scale-up. *J. Pharmacokinet. Biopharm.* **1**, 435–461 (1973).

21. Deng, R. *et al.* Projecting human pharmacokinetics of therapeutic antibodies from nonclinical data: what have we learned? *MAbs.* **3**, 61–66 (2011).

22. Kappos, L. *et al.* Ocrelizumab in relapsing-remitting multiple sclerosis: a phase 2, randomised, placebo-controlled, multicentre trial. *Lancet* **378**, 1779–1787 (2011).

23. Akaike, H. A new look at the statistical model identification. *IEEE Trans. Automat. Controls* **19**, (1974).

24. Smith, E.J. *et al.* A novel, native-format bispecific antibody triggering T-cell killing of B cells is robustly active in mouse tumor models and cynomolgus monkeys. *Sci. Rep.* **5**, 17943 (2015).

25. Schlereth, B. *et al.* T-cell activation and B-cell depletion in chimpanzees treated with a bispecific anti-CD19/anti-CD3 single-chain antibody construct. *Cancer Immunol. Immunother.* **55**, 503–514 (2006).

26. Chichili, G.R. *et al.* A CD3xCD123 bispecific DART for redirecting host T cells to myelogenous leukemia: preclinical activity and safety in nonhuman primates. *Sci. Transl. Med.* **7**, 289ra282 (2015).

27. Trivedi, A. *et al.* Clinical pharmacology and translational aspects of bispecific antibodies. *Clin. Transl. Sci.* **10**, 147–162 (2017).

28. Press, O.W. *et al.* Monoclonal antibody 1F5 (anti-CD20) serotherapy of human B cell lymphomas. *Blood* **69**, 584–591 (1987).

29. McLaughlin, P. *et al.* Rituximab chimeric anti-CD20 monoclonal antibody therapy for relapsed indolent lymphoma: half of patients respond to a four-dose treatment program. *J. Clin. Oncol.* **16**, 2825–2833 (1998).

30. Maloney, D.G. *et al.* IDEC-C2B8 (Rituximab) anti-CD20 monoclonal antibody therapy in patients with relapsed low-grade non-Hodgkin's lymphoma. *Blood.* **90**, 2188–2195 (1997).

31. Goede, V. *et al.* Obinutuzumab plus chlorambucil in patients with CLL and coexisting conditions. *N. Engl. J. Med.* **370**, 1101–1110 (2014).

32. Struemper, H. *et al.* Population pharmacokinetics of ofatumumab in patients with chronic lymphocytic leukemia, follicular lymphoma, and rheumatoid arthritis. *J. Clin. Pharmacol.* **54**, 818–827 (2014).

33. Hagenbeek, A. *et al.* First clinical use of ofatumumab, a novel fully human anti-CD20 monoclonal antibody in relapsed or refractory follicular lymphoma: results of a phase 1/2 trial. *Blood* **111**, 5486–5495 (2008).

34. Edwards, J.C. *et al.* Efficacy of B-cell-targeted therapy with rituximab in patients with rheumatoid arthritis. *N. Engl. J. Med.* **350**, 2572–2581 (2004).

35. Ng, C.M., Bruno, R., Combs, D. & Davies, B. Population pharmacokinetics of rituximab (anti-CD20 monoclonal antibody) in rheumatoid arthritis patients during a phase II clinical trial. *J. Clin. Pharmacol.* **45**, 792–801 (2005).

36. OcrevusTM [package insert]. **2nd April**.

Supplementary information accompanies this paper on the *Clinical and Translational Science* website.
(www.cts-journal.com)